New Journal and we have not received input yet 34 (2022) 101429

Contents lists available at ScienceDirect

Thermal Science and Engineering Progress

journal homepage: www.sciencedirect.com/journal/thermal-science-and-engineering-progress

Experimental study on silica gel/ethanol adsorption characteristics for low-grade thermal driven adsorption refrigeration systems

Ahmed Rezk [a,b,*], Gamze Gediz Ilis [c], Hasan Demir [d]

[a] Energy and Bioproducts Research Institute (EBRI), College of Engineering and Physical Science, Aston University, Birmingham B4 7ET, UK
[b] Aston Institute of Material Research (AIMR), College of Engineering and Physical Science, Aston University, Birmingham B4 7ET, UK
[c] Department of Mechanical Engineering, Gebze Technical University, Turkey
[d] Department of Chemical Engineering, Osmaniye Korkut Ata University, Turkey

ARTICLE INFO

Keywords:
Adsorption cooling
Silica gel/Ethanol
Adsorption characteristics
Refrigeration

ABSTRACT

There has been an increasing interest in adsorption cooling and heat pumps as the most feasible green alternative to the widespread vapor compression technology. Recent developments in adsorption cooling highlighted the need for cost-efficient adsorption pairs of advanced adsorption characteristics. In response, this article experimentally investigates and models silica gel/ethanol pair adsorption characteristics that can utilize low-temperature heat sources, such as those available in the emerging electric vehicles and PV/T systems. The investigated characteristics are the porous structure stability, isosteric heat of adsorption, adsorption diffusion energy, adsorption isotherm, and adsorption kinetic under extended operating conditions 15–55 °C. The results showed the high affinity of silica gel towards ethanol to provide sub-zero cooling. Silica gel showed no structure deterioration during the repetitive adsorption/desorption cycles of net 22 % cyclic ethanol uptake. The chemical adsorption of silica gel/ethanol showed a high level of adsorption/desorption reversibility with minimal hysteresis, which the Langmuir model best simulated. The heat of adsorption was determined to be 4.49×10^4 J/mol, which was higher than the diffusion energy of 1.80×10^4 J/mol due to the slow physical mobility of ethanol molecules inside silica gel pores. The Elovich kinetic model was the most suitable for simulating the chemical adsorption/desorption processes. The material level cyclic analysis showed the potential of 22 kJ/kg_{ads} cooling effect and 0.97 coefficient of performance by utilizing a 55 °C heat source, widely available in PV/T systems and electric vehicles.

1. Introduction

The Paris Agreement entered into force in 2016 and was signed by 200 countries to reduce global warming to below 2 °C, primarily by reducing greenhouse gas emissions. In 2021, COP 26 conference was held to accelerate the countries' plans to achieve such a goal. Reducing greenhouse gas emissions can be supported by using environmentally friendly cooling and heat pump systems. Adsorption cooling (AdC) is one of the most promising technologies for cooling and heat pump systems that could improve the life of people due to using environmentally friendly refrigerants, operating with low-temperature thermal energy sources (80–150 °C), such as geothermal, solar thermal, and heat wasted from many industrial processes [1–4]. Heat sources above 90 °C can be utilized by a wide range of adsorption working pairs. However, the currently available pairs are unlikely to utilize heat sources below 50 °C [5]. Current AdC systems either cannot operate at such low temperatures, or their performance drops considerably. For this reason, the researchers are working on new adsorbents to improve the AdC performance.

Given the stability of ethanol adsorbate (i.e., refrigerant) and its potential to provide sub-zero cooling in AdC, many researchers have investigated its utilization with different porous adsorbents. Denzinger et al. [6] investigated ethanol/activated carbon pairs for small bench-scale prototype adsorption refrigeration that worked at temperatures between 2 °C and 8 °C. El-Sharkawy et al. [7] developed new adsorbents from potassium hydroxide treated with spherical phenol resin with varied mass ratios to operate with ethanol as an adsorbate: KOH4-PR and KOH6-PR. The ethanol adsorption onto KOH4-PR and KOH6-PR was 1.43 kg/kg_{ads} and 2 kg/kg_{ads}, respectively. Rezk et al. [8] studied

* Corresponding author at: Department of Mechanical, Biomedical and Design Engineering, College of Engineering and Physical Science, Aston University, Birmingham B4 7ET, UK.
E-mail addresses: a.rezk@aston.ac.uk (A. Rezk), ggedizilis@gmail.com (G. Gediz Ilis), hasandemir@osmaniye.edu.tr (H. Demir).

https://doi.org/10.1016/j.tsep.2022.101429
Received 27 April 2022; Received in revised form 1 July 2022; Accepted 16 July 2022
Available online 25 July 2022

Nomenclature

a	Initial adsorption rate constant of the Elovich model (kg/kg/s)
A	Polanyi potential
AdC	Adsorption chiller
b	Adsorption/Desorption rate constant of the Elovich model (kg/kg)
COP	Coefficient of performance
D	diffusivity, m^2/s
D_{eff}	Effective diffusivity (m^2/s)
Δq	Uptake difference (kg/kg)
DVS	Dynamic vapor sorption
E	Diffusion energy, (kJ/mol)
E_a	heat of adsorption, J/mol
EV	Electrical vehicle
h_{fg}	Evaporation/condensation heat of ethanol (kJ/kg)
k_1	the equilibrium rate constant of pseudo-first-order adsorption, 1/s
K_{DR}	Dubinin-Radushkevich constant, mol^2/kJ^2
K_f	Sorption capacity, 1/kPa
K_L	Langmuir constant, (1/kPa)
K_T	Tóth isotherms constant
M	Molecular weigh (kg/mol)
n	eigenvalue used in Freundlich model, and Tóth model
P	Pressure, kPa
PV/T	Photovoltaic thermal panel
q_∞	the amount of adsorbate at equilibrium, kg_{EtOH}/kg_{ads}
q_e	Adsorbate amount at equilibrium, kg_{EtOH}/kg_{ads}
q_m	Adsorbate amount when monolayer, kg_{EtOH}/kg_{ads}
q_t	the amount of adsorbate at any time, kg_{EtOH}/kg_{ads}
R	Universal gas constant, J/(mol K)
R_p	particle radius of adsorbent, m
T	temperature, K
t	time, s

Subscripts

0	reference
ads	Adsorbent
bed	adsorbent bed
cond	condenser
e	equilibrium
eff	effective
EtOH	Ethanol
evap	evaporator
s	saturation

ethanol adsorption onto six different MOFs: MIL-101Cr, MIL-100Cr, MIL-53Cr, CPO-27-Ni, Cu-BTC, and Fe-BTC. The most promising adsorbent was MIL-100Cr, as ethanol's adsorption/desorption processes showed no deterioration for MIL-101Cr structure over 20 successive cycles, and the reported maximum adsorption capacity was 1.2 kg/kg_{ads}. The adsorption heat pump's numerical simulation resulted in the evaporator being close to −15 °C, and the refrigerant outlet temperature was calculated as −7 °C. El-Sharkawy et al. [9] investigated the treated and untreated activated carbon/ethanol adsorption behavior. The maximum ethanol adsorption capacity was achieved by H2-treated Maxsorb III (1.23 kg/kg_{ads}) compared to the untreated Maxsorb III (1.2 kg/kg_{ads}), and KOH-H2 treated Maxsorb III (1.01 kg/kg_{ads}) adsorbents. El-sayed et al. [10] numerically investigated the influence of adsorbent particle thickness of Maxsorb activated carbon on ethanol adsorption and the bed temperature. Increasing the adsorbent's thickness above 10 mm increased the initial bed's temperature and reduced the adsorption uptake of ethanol. Adsorbent thicknesses below 10 mm showed a higher uptake performance, and consequently, better cooling performance was reported. Cui et al. [11] studied ethanol adsorption and refrigeration capacities of two in-house developed adsorbents, NA and NB. The ethanol adsorption capacities of adsorbents NA and NB were 0.7 kg/kg_{ads} and 0.68 kg/kg_{ads}, respectively. The refrigeration capacities of adsorbent NB ranged from 274 to 452 kJ/kg for different desorption temperatures. Li et al. [12] constructed an adsorption ice maker working with activated carbon ethanol pair, and the reported COP was 0.034. Askalany et al. [13] reviewed the adsorption chiller employing activated carbon adsorbent. The COP of the activated carbon/ethanol pair used adsorption chiller was 0.8.

To follow up on the development at the material level, several scientists devoted their efforts to developing sorption composites by either blending the conventional porous adsorbents with heat transfer enhancers or impregnating metal salts into a hosting matrix to intensify the sorption characteristics. Rocky et al. [14] recently reviewed the development of porous/thermal enhancer/binder composites, including their use with ethanol for low-temperature applications. Generally, the thermal enhancer element contributed considerably to the adsorption kinetics due to the enhanced thermal response. Grekova et al. [15] developed a sorption composite from LiCl and the state-of-the-art multiwalled graphene nanotubes and studied their characteristics but with methanol for a low-temperature heat-storing application area. These studies give examples of the future direction for the development at the material level.

Using the low-temperature heat sources enables broadening the AdC's application areas. Previous studies have reported that AdC for vehicles air conditioning, photovoltaic/thermal (PV/T) panels, and other combined cycles are the most prominent application areas that require low-temperature heat sources [16–20]. On reflection, Calis et al. [21] investigated the techno-economic of zeolite/water adsorption chiller system assembled by PVT collectors. With the adsorption cooler's cooling effect, the PV panels' electrical efficiency has been increased by 16 %. Furthermore, Gagliano et al. [16] analyzed the performance difference between cooling PV modules with vapor compression and silica gel/water AdC systems. As a result, PV/*T*-AdC produced about 2.3 kWh/d (0.264 kWh/kW) during a typical day and even 4.5 kWh (0.515 kWh/kW) during the peak day.

In recent years, several studies have used AdC in vehicle cabin cooling as an environmentally friendly alternative [22]. Maeda et al. [23] recently reviewed the articles on using AdC in fossil fuel-powered cars. It was concluded that while the fuel economy of the AdC-cooled cars decreased by 1 %, the vapor compression compressor-cooled cars' fuel economy decreased by 8 %. Ali and Chakraborty [24] provided 3 kW of cooling in the vehicle cabin by utilizing the exhaust waste heat of a 3-liter six-cylinder car. According to the experiments, the coefficient of performance (COP) of the AdC utilizing 8 kg of $CaCl_2$-silica gel adsorbent was 0.39, and the specific cooling power (SCP) was 0.52 kW/kg with a cycle time of 500 s. Verde et al. [25,26] developed AdC employing waste heat of Fiat Grande Punto 1.9 JTD engine; the AdC weighed 86 kg. The amount of waste heat generated from the engine under road conditions was sufficient to operate the AdC system, showing an average COP and cooling capacity of 0.35 and 2.1 kW. Verde et al. [27] simulated the adsorbent bed of the AdC produced for Grande Punto and optimized the geometric dimensions of the bed. The COP was increased from 0.35 to 0.55 by increasing the pipe pitch in the adsorbent bed from 4 mm to 0.8 mm. Vasta et al. [28] developed an AdC of 170 dm^3 volume that weighed 60 kg for the IVECO STRALIS truck to utilize the engine waste heat. The desorption temperature of 90 °C generated a cooling power of 2.3 kW, and a COP of 0.45 was obtained. Verde et al. [29] developed AdC of 5 kW cooling power and 0.6 COP using 80–90 °C

truck engine waste heat. According to the literature above, AdC can be exploited efficiently in fossil-fueled (i.e., internal combustion engines operated) automobiles and trucks' air conditioning.

Given the revolutionized automotive industry, electric vehicles (EV) will dominate the market in the coming few decades; thus, the use of fossil fuel exhaust gases for AdC will be no longer available. The significant heat sources in EVs are the electric battery and motor electromagnetism. Besides, the demand for PV/T increases, not only for hot climates. A significant challenge with these application areas is the low-temperature heat to drive AdC that most likely falls below 50 °C. With the emphasis on sub-50 °C benchmark, integrating AdC with next-generation technological advances (e.g., electric vehicles and PV/T) can only be possible if new adsorption pairs can be developed. Therefore, Habash et al. [30] devoted their research effort to developing AdC utilizing silica gel/ethanol pair operated by sub-50 °C heat sources, but this study was limited to a single operating condition.

Given the literature above, what is not yet clear is the influence of different operating conditions on silica gel/ethanol characteristics to efficiently utilize it in the EV and PV/T application areas that generate low-temperature heat. Therefore, the novelty of this paper is experimentally investigating silica gel/ethanol pair's adsorption characteristics and empirically modeling such characteristics under extended operating conditions 15–55 °C to cover the identified knowledge gap. Silica gel structure stability, adsorption isotherm, adsorption kinetic, isosteric heat of adsorption, adsorption diffusion energy, and the theoretical cyclic performance at the material level were experimentally determined by employing thermal-gravimetrical measured sorption isotherms and kinetics. The results contribute to the knowledge by providing critical insight into silica gel/ethanol adsorption, including the theoretical cyclic performance at the material level, as a promising pair for cost-efficient sub-zero cooling applications.

2. Material and methods

The silica gel was a Fuji RD type bead supplied by Fuji Silysia Chemical (Japan). The diameter of the adsorbent bead is 2.2 mm. The BET surface area was 820 m^2/g, and the average pore size of the silica gel was 2.2 nm. Ethanol (Ethyl alcohol C_2H_6O) 99+% was obtained from ThermoFisher Scientific and used as a sorbate (i.e., refrigerant).

The sorption characteristics of the Fuji silica gel/ethanol pair were determined using the dynamic vapor sorption (DVS) gravimetric analyzer DVS Resolution™ by Surface Measurements Systems, as shown in Fig. 1. The change in the adsorbent mass is measured using a microbalance (SMS Ultrabalance™) of high long-term stability at the microgram level as it adsorbs the selected vapor (i.e., solvent) at a controlled pressure ratio equivalent to P_{evap}/P_{bed}. Dry nitrogen is used to automatically purge the balance and reaction chambers before sample loading to prevent the vapor condensation in the balance chamber. A proprietary Speed of Sound sensor measures and controls via PID mass flow controllers the ethanol (i.e., organic vapor – solvent 2) generation. If water vapor is used (solvent 1), an RH sensor is used to control the vapor generation via the PID mass flow controllers. The accuracy of the DVS analyzer microbalance was verified ± 0.05 mg by using 100 mg standard calibration mass before test execution. The determined sorption characteristics included adsorption isotherms, adsorption kinetics, and adsorption heat.

Fresh samples of Fuji silica gel were placed in the reaction chamber of the DVS for every test that was locally dried by a heater at a fixed temperature of 55 °C until no change of the mass condition was reached; it usually took 5 h. The mass at the end of the drying process was considered the dry mass (i.e., reference mass) for the following test to maintain the consistency of pre-testing sample conditions. The drying process followed adsorption/desorption tests at various pressure ratios, equivalent to P_{evap}/P_{bed} during adsorption and P_{cond}/P_{bed} during desorption, and temperatures to develop the required characteristic curves. The sample masses were recorded every 1 min to determine the adsorption kinetics at the predefined temperature and pressure ratio. It is noteworthy that the utilizing nitrogen as a carrier gas for the adsorbate vapor during the adsorption/desorption processes, as the effect of carrier gas on the adsorption kinetics is less than 10 %, as reported by Rezk et al. [8].

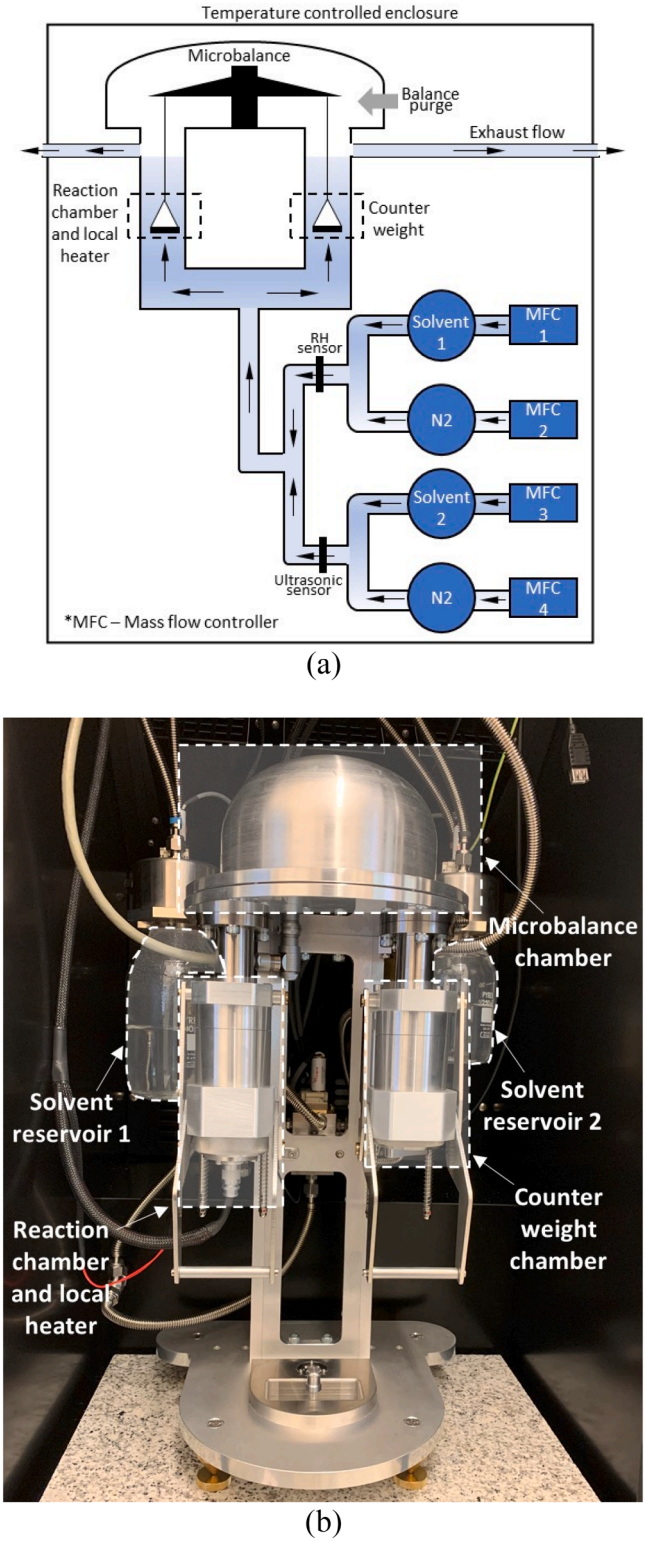

Fig. 1. Dynamic Vapor Sorption Analyzer (a) schematic diagram and (b) pictorial view.

3. Results and discussion

This section presents the experimental investigation of silica gel/ethanol adsorption characteristics through thermal-gravimetrical experiments. Adsorption isotherms, adsorption kinetics, and the impact of regeneration temperature on the desorption rate and the non-desorbed ethanol due to the high porosity of silica gel were determined under the temperature range of 15–55 °C. Moreover, Silica gel structure stability, the isosteric heat of adsorption, and adsorption diffusion energy were determined. Determining silica gel/ethanol characteristics eventually enabled determining the pair's potential specific cooling capacity and COP at the material level.

3.1. Structure stability

Fig. 2 shows repeatability gravimetrical test results of adsorption/desorption processes of ethanol/silica gel pair. The ethanol vapor pressure ratio in the medium was alternated between 90 % and 0 % at 25 °C. It can be observed that no loss in the Ethanol uptake exists over ten consecutive adsorption/desorption cycles. The ethanol uptake varied from 12 % to 34 % for all cycles, representing 22 % net cyclic uptake for the given pressure ratio swing, but the adsorption rate was considerably faster than desorption. The fast adsorption rate indicates the high affinity of silica gel towards ethanol vapor. The slower desorption rate results from the high microporosity of Fuji silica gel that slows the intraparticle mass transfer of ethanol of a relatively large molecule size of 0.44 nm if compared, for instance, to that of 0.28 nm for water. This test reveals the repeatability of ethanol vapor adsorption/desorption on/from silica gel and the stability of silica gel structure, while the scientific consensus tended towards the potential deterioration of silica gel due to ethanol adsorption/desorption [8,10,11].

3.2. Adsorption isotherms analysis

Fig. 3 depicts the temporal change of the ethanol uptake at different pressure ratios (P_e/P_s) 0–90 % and temperatures of 15–55 °C during adsorption and desorption. At the end of each P_e/P_s step, the equilibrium uptake was recorded to generate the corresponding adsorption/desorption isotherm. The amount of adsorbed ethanol reached 30–32 %, with 56–62 % of the maximum uptake occurring at a P/P of 10 % for all temperatures. The large percentage of the adsorption uptake at low P_e/P_s highlights the high affinity of Fuji silica gel towards ethanol. A distinct difference during adsorption processes was that the time consumed to reach the maximum uptake at P_e/P_s of 90 % decreases with increasing sorption temperature. Increasing the sorption temperature quantitively increased the desorption amount of ethanol from silica gel particles, reducing the non-desorbed amount of ethanol from silica gel particles. At 15 °C, 12.4 % ethanol was not desorbed from silica gel. These non-desorbed amounts vary as 10.9 %, 8.6 %, 7.2 %, and 5.8 % ethanol for 25, 35, 45, and 55 °C, respectively.

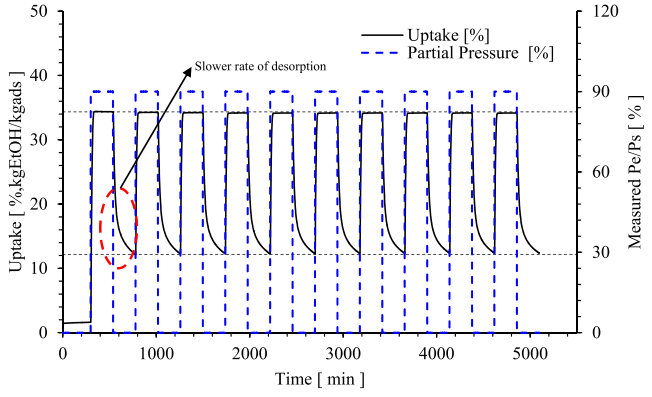

Fig. 2. Repeatability test of ethanol-silica gel pair.

Generally, hysteresis is caused by capillary condensation of adsorbate in the mesopores and can be observed in adsorption/desorption isotherms. The adsorption/desorption hysteresis for the ethanol/silica gel pair is shown in Fig. 4. The maximum hysteresis of 1.01 % was observed at the P_e/P_s 50–60 % region, resulting from ethanol condensation inside silica gel pores. Except for such small hysteresis, adsorption and desorption behaviors overlapped, reflecting the high adsorption/desorption reversibility level. El-Sharkawy et al. [7] also observed similar behavior for the ethanol/KOH-PR pair.

The adsorption isotherms of the silica gel/ethanol pair are presented in Fig. 5. The maximum adsorption capacity was 32 % kg_{EtOH}/kg_{ads} at 15 °C adsorption temperature. The increment of adsorption temperature caused decreased adsorption capacity at low ethanol pressure. However, at the high partial pressure of ethanol, the adsorption capacity reached 30 % for all temperatures. The maximum adsorption capacities for 25, 35, 45, and 55 °C were 30.97, 30.44, 31.63, and 29.65 % kg_{EtOH}/kg_{ads}, respectively.

The isotherms of ethanol-silica gel adsorption were modeled by Langmuir, Freundlich, Dubinin-Radushkevich, and Tóth's equations [31–33]. The Langmuir model was expressed in the literature, as shown in equation (1).

$$\frac{q_e}{q_m} = \frac{K_L P_e}{1 + K_L P_e} \tag{1}$$

The Langmuir constant was symbolled with K_L (1/kPa), and partial pressure of ethanol at equilibrium was implied by P_e (kPa). The symbols q_e and q_m represent the adsorption amount at equilibrium and the maximum monolayer adsorption amount (kg/kg_{ads}) [31]. The slope of the $\frac{P_e}{q_e}$ vs P_e linear curve gives $1/q_m$, and intercept of linear curve equals to $\frac{1}{q_m K_L}$. Thus, the constants q_m and K_L can be found linear form of Langmuir model.

The non-linear Freundlich isotherm model can be expressed by equation (2).

$$q_e = K_f P_e^{1/n} \tag{2}$$

A sorption capacity was denoted with K_f (1/kPa). A sorption intensity was symbolled with n. The linear form of Freundlich isotherms was obtained by drawing log qe versus log Pe. The slope of the linear curve gives 1/n, and the intercept of the linear curve equals log(K_f). When n equals 1, the adsorption is in linear form. When n is bigger than 1, it can be interpreted as adsorption is favorable, and the increment of adsorbed amount decreases with increasing adsorptive concentration. When n is smaller than 1, the adsorption is unfavorable, and the increment of adsorbed amount increases with the increasing concentration of adsorptive [32].

The Dubinin-Radushkevich isotherm accepts that the pore volume filling mechanism adsorption onto heterogeneity surface energy. The Dubinin-Radushkevich isotherm model can be expressed using equations 3–5 [34,35].

$$q_e = q_m exp\left(-K_{DR} A^2\right) \tag{3}$$

$$A = RTln\left(\frac{P_s}{P_e}\right) \tag{4}$$

$$E_a = 1/\sqrt{K_{DR}} \tag{5}$$

The Dubinin-Raduskevich constant related to adsorption energy was denoted with K_{DR} (mol^2/kJ^2); R is the universal gas constant (J/(mol K)); A is Polanyi potential; E is mean adsorption energy (kJ/mol) [35]. The linear form of Dubinin-Radushkevich isotherm was obtained by drawing ln(q_e) versus A^2. This line's intercept equals ln(q_m), and the slope gives the minus K_{DR}.

The Tóth isotherm was a modified form of Langmuir isotherms and expressed as follows. When the n equals 1, the equation returns to the

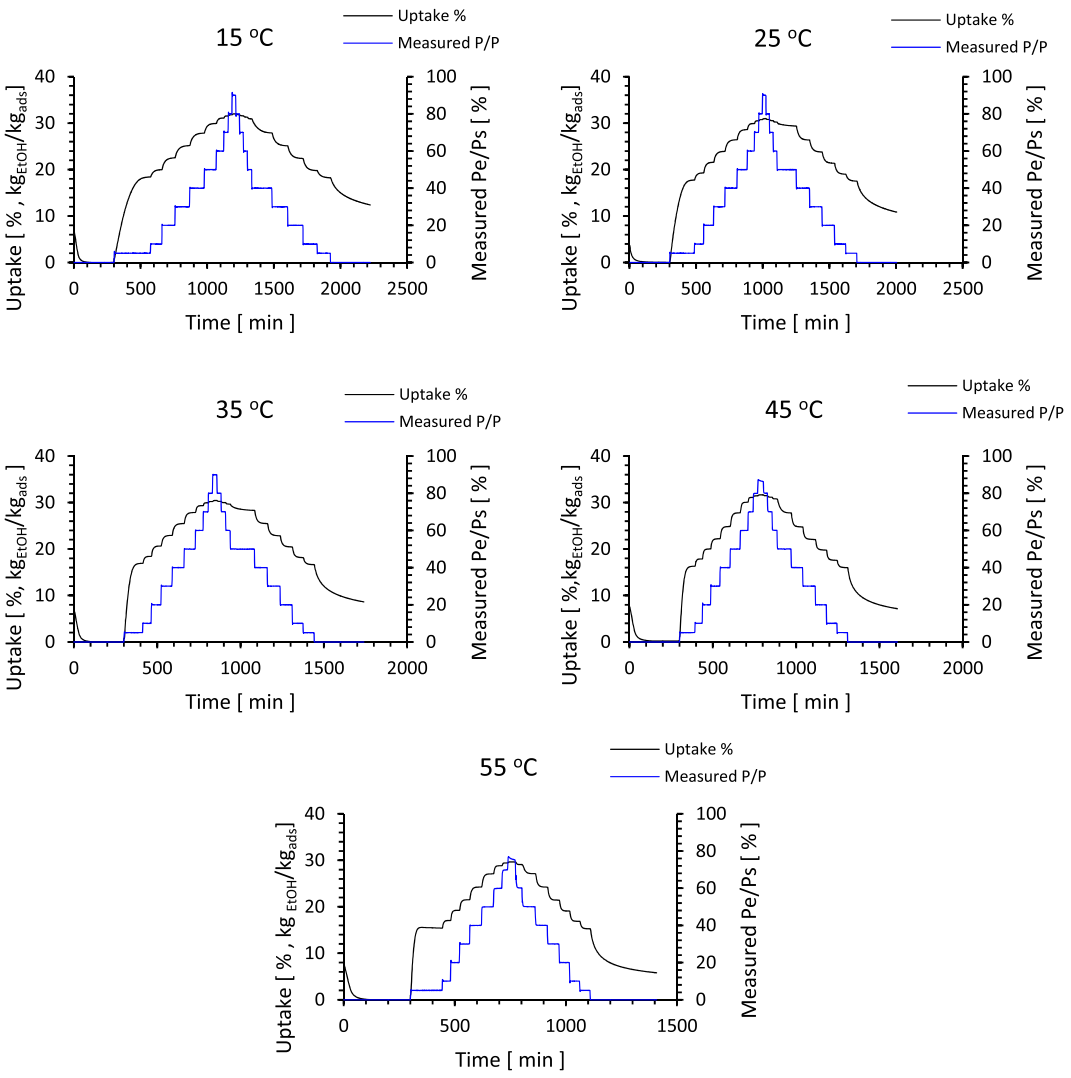

Fig. 3. Temporal change of the ethanol uptake at different sorption temperatures.

Langmuir isotherm equation.

$$\frac{q_e}{q_m} = \frac{K_T P_e}{\left[1 + (K_T P_e)^n\right]^{1/n}} \tag{6}$$

K_T and n are the Tóth isotherm constants [32].

Table 1 lists the constants of Langmuir, Freundlich, Dubinin-Raduskevich, and Tóth isotherms at different adsorption temperatures and their regression coefficients. The regression coefficients indicate the best fitting isotherms to experimental data. The results show that the regression coefficients of Langmuir and Tóth isotherm models were relatively higher than Freundlich and Dubinin-Radushkevich's isotherm models. The abovementioned Tóth isotherm model is modified of the Langmuir isotherm model. Both isotherm equations can simulate ethanol/silica gel adsorption isotherms over a wide range of operating temperatures. The Langmuir isotherm model assumes that the adsorption occurs on homogeneous surfaces with monolayer adsorption [31]. Freundlich isotherm constant "n" was calculated as nearly 4. The interpretation of this situation was that ethanol adsorption onto silica gel was favorable. The ethanol adsorption on silica gel shows similar behavior, as the amount of adsorption decreases with the increasing concentration of the adsorbate [32]. This agrees with the assumption of the Langmuir isotherm model, which was monolayer adsorption. The mean adsorption energy I in the Dubinin-Raduskevich isotherm model represents and describes the adsorbate-adsorbent interaction. When the magnitude of mean adsorption energy is smaller than 8 kJ/mol, the adsorption process can be classified as physical adsorption, and when the E value is between 8 kJ/mol and16 kJ/mol, the adsorption can be classified as chemical adsorption [35]. For all adsorption temperatures, the E was calculated as 10 kJ/mol, denoting that the adsorption process of silica gel/ethanol is chemical adsorption. As shown in Fig. 5, the maximum adsorption capacities were nearly constant against the adsorption temperatures. This behavior confirms that ethanol adsorption onto silica gel was chemical, not physical adsorption.

Fig. 6 represents the four isotherm models against the experimental adsorption isotherms at different temperatures. The four isotherm models' non-linear form was drawn using their calculated constants. The Tóth isotherm model does not perfectly fit the experimental data at the low vapor pressure of ethanol. On the other hand, the Langmuir and Freundlich isotherms models demonstrated the best fit at ethanol's low and high vapor pressures. In addition, the maximum adsorption capacities in the Tóth model were closer than those of the Freundlich model. However, Freundlich isotherms show a better fit for all vapor pressure of ethanol than Tóth isotherms. Hence, taking in the count for both regression coefficients and Fig. 6, the order of the best-fitting isotherms to experimental data can be ordered as (1) Langmuir; (2) Freundlich; (3) Tóth; (4) Dubinin-Radushkevich. Chen [33] also used a similar technique to determine the best fitting isotherm for their experimental adsorption data.

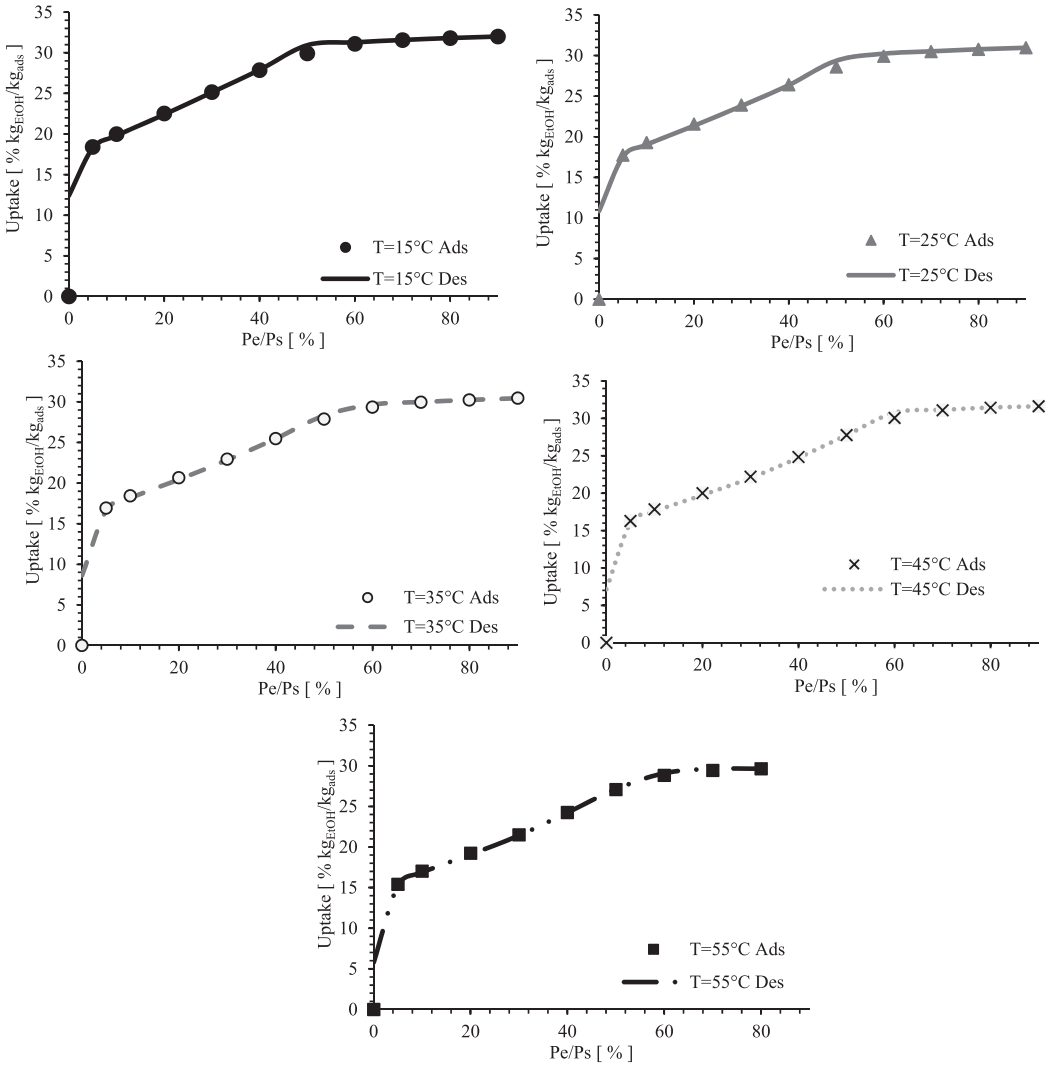

Fig. 4. Adsorption/desorption isotherm of silica gel – ethanol pair for different temperatures.

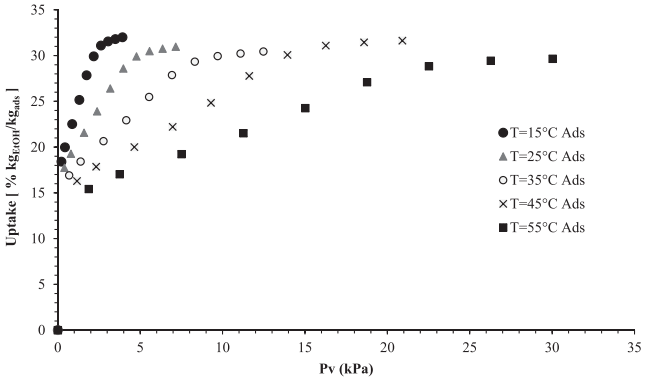

Fig. 5. Adsorption isotherms of ethanol/silica gel pair.

Tóth model statistically showed the highest R-squared value, which resulted from the region of underestimating the equilibrium uptake at low vapor pressure that was balanced out by more points overestimating it at higher vapor pressure; this is throughout the investigated temperature range. However, the Tóth model cannot be physically regarded as the best fit from the adsorption isotherm viewpoint. Langmuir and Freundlich, therefore, succeeded the Tóth model physically, considering R-squared statistical value to promote Langmuir over Freundlich.

3.3. Adsorption diffusivity analysis

Fig. 7 depicts the temporal equilibrium uptake of ethanol onto silica gel, which is used to determine the ethanol vapor diffusivity inside silica gel pores. As aforementioned, the ethanol adsorption process was determined to be chemical adsorption, and this phenomenon was also observed in Fig. 7, as the adsorption temperature did not affect the maximum equilibrium adsorption uptake of silica gel. Equation (7) represents the one-dimensional unsteady isothermal diffusion mass transfer for a spherical particle [7]. To match the theory, the inside and outside temperatures of the silica gel particle should be at equilibrium.

$$\frac{q_t}{q_\infty} = 1 - \frac{6}{\pi^2}\sum_{n=1}^{\infty}\frac{1}{n^2}exp\left[-\frac{n^2\pi^2 D_{eff}t}{R_p^2}\right] \tag{7}$$

The radius silica gel particle was denoted with R_p, which equals 1.1 mm. The D_{eff} represents the effective diffusivity of the ethanol through the silica gel pores. Equation (8) was valid when q_t/q_∞ is higher than 0.7. This region was called the long-term region. The linear form of equation (8) was plotted by $ln(1-q_t/q_\infty)$ versus t. The effective diffusivity of ethanol vapor through the silica gel particle for the long-term region can be found from the slope $\left(-\frac{\pi^2 D_{eff}}{R_p^2}\right)$.

Table 1
Adsorption isotherms models constants for ethanol – silica gel pair.

Isotherm Model	Constants	Adsorption Temperatures				
		15°C	25 °C	35 °C	45 °C	55 °C
Langmuir	q_m	35	33.9	33.6	35.7	33.4
	K_L	2.72	1.42	0.74	0.34	0.23
	R^2	0.9951	0.9938	0.9920	0.9938	0.9833
Freundlich	K_f	24.5	20.6	17.4	14.06	12.3
	n	4.67	4.66	4.4	3.98	3.87
	R^2	0.9755	0.9739	0.9705	0.9578	0.9624
Dubinin – Radushkevich	K_{DR}	$1x10^{-8}$	$1x10^{-8}$	$1x10^{-8}$	$1x10^{-8}$	$1x10^{-8}$
	E	10	10	10	10	10
	q_m	30.27	29.06	28.35	28.74	27.17
	R^2	0.8741	0.8595	0.8491	0.8132	0.8364
Tóth	q_m	32.2	32.2	32.2	32.2	31.6
	K_T	0.8	0.4	0.2	0.1	0.1
	n	3	3	3	3	4
	R^2	0.9980	0.9971	0.9962	0.9909	0.9932

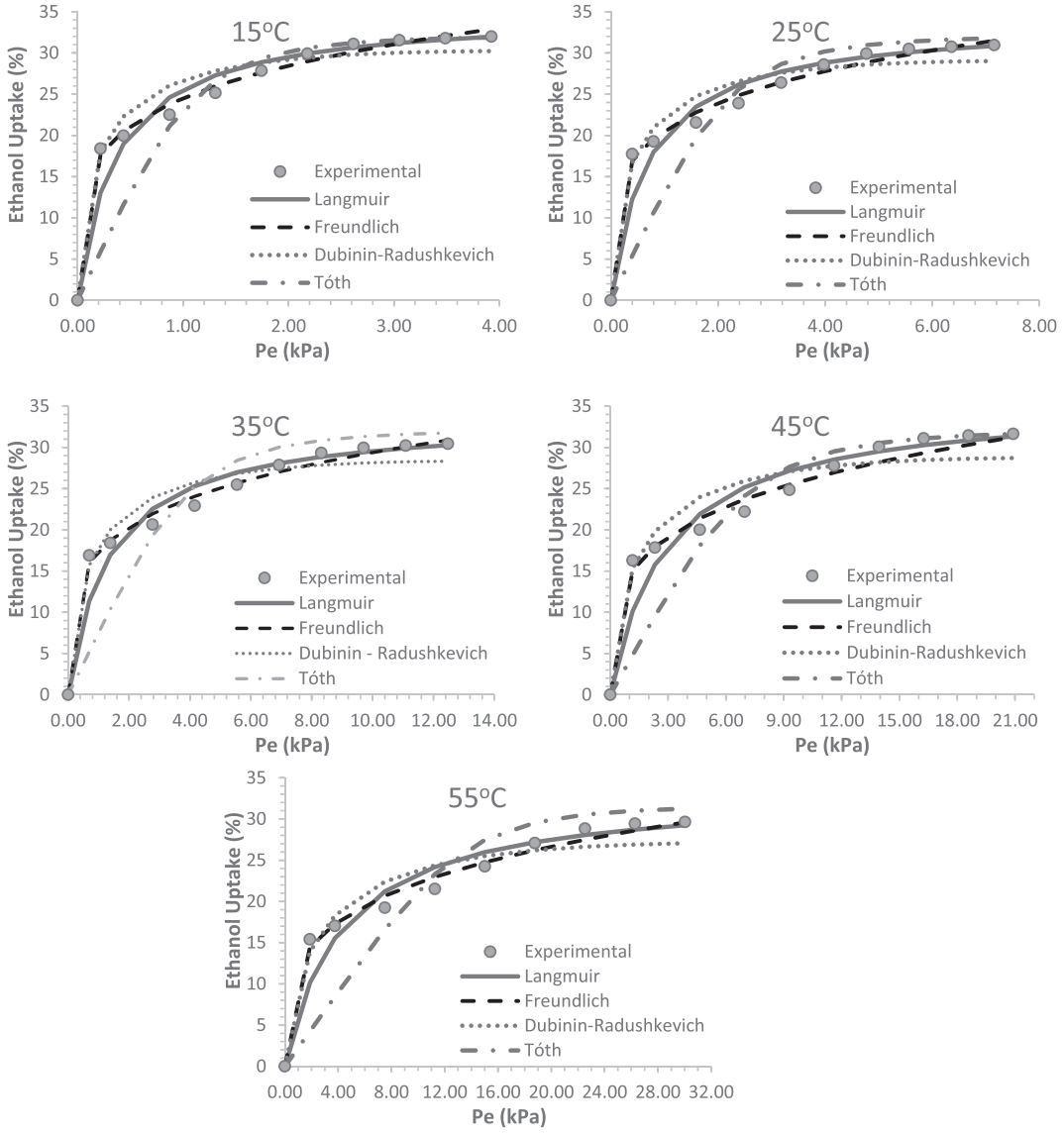

Fig. 6. The experimental Langmuir, Freundlich, Dubinin-Radushkevich, and Tóth adsorption isotherms of ethanol/silica gel pair.

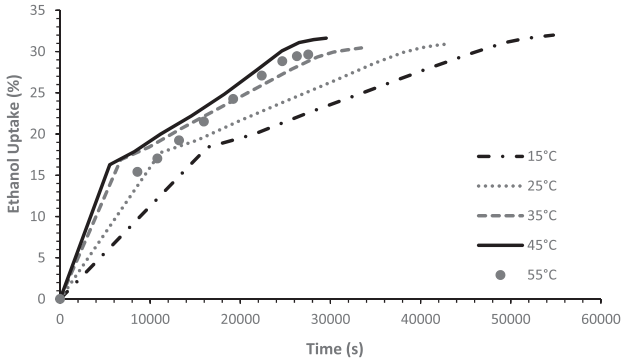

Fig. 7. Temporal equilibrium uptake of ethanol adsorption on silica gel at different temperatures.

Table 2
Ethanol diffusivity on silica gel particle against temperature.

T (°C)	D_{eff} (m^2 s^{-1})	R^2	E (J mol^{-1})	D_0 (m^2 s^{-1})	R^2
15.0	1.73E-11	0.8768	17,956	2.92E-8	0.9669
25.0	2.00E-11	0.8795			
35.0	2.39E-11	0.8934			
45.0	3.42E-11	0.8852			
55.0	4.16E-11	0.8855			

$$\frac{q_t}{q_\infty} = 1 - \frac{6}{\pi^2} exp\left[-\frac{\pi^2 D_{eff} t}{R_p^2}\right] \tag{8}$$

The effective ethanol diffusivities through silica gel pores against adsorption temperatures are populated in Table 2. The diffusivity strongly depends on temperature, which is generally expressed in Arrhenius form on the experimental data, as shown in Equation (9) [7].

$$D_{eff} = D_0 \exp(-\frac{E}{RT}) \tag{9}$$

The D_0 symbolized a reference diffusivity constant, and the activation energy was denoted with E (J mol^{-1}); R is the gas constant. The linear form of equation (9) was obtained by plotting $\ln(D_{eff})$ versus 1/T. The activation energy can be found from the slope of this linear curve, and the reference diffusivity was calculated from the curve intercept. The calculated E and D_0 are given in Table 2 with a regression coefficient of 0.9834.

3.4. Isosteric heat of adsorption

The heat of adsorption quantifies the exothermic/endothermic energies in joules developed during the adsorption/desorption of each mole of ethanol. The heat of adsorption was determined using the Clausius-Clapeyron-type equation, and the relation between the heat of adsorption and surface coverage measured by the change in adsorbent mass due to the ethanol uptake is shown in Fig. 8. The Clausius-Clapeyron-type equation was solved by assuming an exclusively exothermic adsorption process at 10 points along the isotherms at two adsorption temperatures to match the theory: $T_1 = 20$ °C and $T_2 = 40$ °C. The average heat adsorption value of 4.49×10^4 J/mol was determined, and the standard deviation was 1.92×10^3 J/mol. Equations (10) and (11) present the deferential and integral forms of the Clausius-Clapeyron-type equation at two temperatures, T_1 and T_2, and their corresponding pressure ratios $(P/P_{bed})_1$ and $(P/P_{bed})_2$. The heat of adsorption is slightly above the heat of vaporization for ethanol of 42.3×10^3 J/mol at 25 °C, indicating multilayer condensation and that not all Ethanol molecules are in contact with the pore surfaces [36]; this aligns with the noticed hysteresis as commented above.

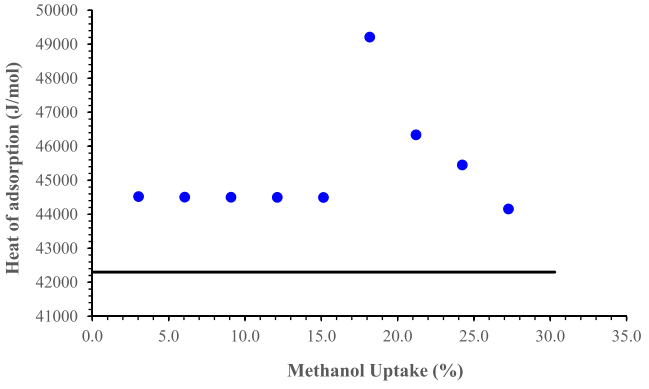

Fig. 8. Plot the isosteric heat of adsorption versus the surface coverage of the ethanol/silica gel pair.

$$\frac{\partial ln(P/P_{bed})}{\partial T} = -\frac{E_a}{RT^2} \tag{10}$$

$$E_a = -R\frac{ln\left(\frac{(P/P_{bed})_1}{(P/P_{bed})_2}\right)}{\frac{1}{T_1} - \frac{1}{T_2}} \tag{11}$$

In Fig. 8, there was a jump between 15 and 25 % of coverage. This situation was observed rarely in the literature [37–39]. This phenomenon was observed in adsorbate adsorption on graphite and occurred due to crystallization of graphite and, in some cases, hypercritical bidimensional fluid mobility in the homogeneous surface of the adsorbent [37,38]. In the current study, the silica gel surface has silanol groups (-Si-OH) as reactive sites and siloxane bridges (Si-O-Si) as unreactive sites. These two groups have the potential to interact with polar and non-polar adsorbates. For the ethanol molecule side, the ethanol has a hydroxyl group (–OH) that the oxygen atom was façade of the adsorption process, ethyl group (–CH2) can be easily attracted by surface atoms of silica gels [40], and hydrogen atoms can interact with oxygen in siloxane bridge [41]. Liu et al. [40] reported that the leading adsorption process by oxygen atoms is more stable than that of ethyl groups. Therefore, the isosteric adsorption may be stable during the mobility of ethanol molecules on the surface of silica gel at low surface coverage. However, due to the increment of ethanol molecules on the surface, the adsorption configuration may become more stable and force ethanol molecules to bind more to oxygen atoms, which can be caused a jump in the isosteric heat of adsorption.

Furthermore, it can be observed that the isosteric heat of sorption is almost double the amount of diffusion energy. According to Sedláček [42], this phenomenon results when the adsorbate molecules move along the capillary walls for a longer time, which is more recognized during the observed slow mobility during the desorption process in Fig. 1. The high chemical affinity of silica gel towards ethanol overcomes such slow mobility during adsorption. The calculated heat of adsorption does not match that developed from isotherm regression using the, which confirms the unsuitability of the Dubinin-Raduskevich model to simulate the adsorption isotherm and ranking it the least favorite.

3.5. Adsorption kinetics

The adsorption kinetics determine the sorbate uptake/off-take rate during the adsorption and desorption processes. Fig. 9 presents the experimental gravimetric ethanol uptake for Fuji silica gel at 25 °C during the pressure ratio swing from 0.0 to 0.9. The uptake rate was predicted utilizing the pseudo-first-order (PFO) model, as shown in equation (12) [34,43]. Although kinetic models are various, PFO is one of the simplest and widely accepted ones to interpret the adsorption kinetics, specifically at a macroscopic level.

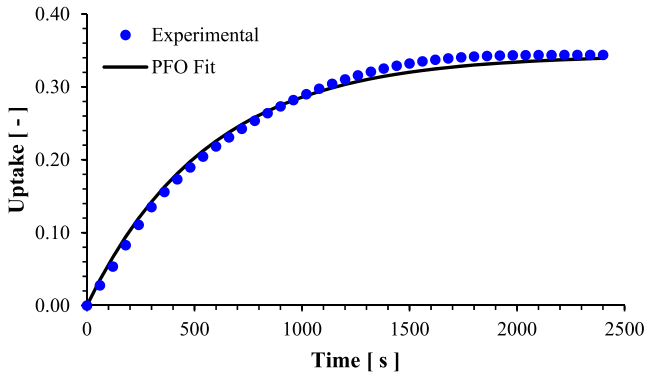

Fig. 9. adsorption kinetic PFO/LDF model compared to the experimental data at 25 °C.

$$q_t = q_e\left(1 - e^{-D_{eff}t}\right) \tag{12}$$

where D_{eff} denotes the rate coefficient (i.e., mass transfer coefficient). PFO is theoretically consistent with the widely known linear-driving-force (LDF) model, as the rate coefficient correlates to the diffusion energy, as shown in equation (9) [44]. The non-linear regression of equation (12) yielded the rate coefficient of $1.78 \times 10^{-3}\ s^{-1}$ and the non-linear regression coefficient was 0.99.

PFO failed to simulate the desorption kinetics. It is not unusual, as PFO is usually well utilized to simulate the physical adsorption/desorption process. Elovich's kinetic model, on the other hand, better simulated the desorption kinetics, as shown in Fig. 10. Accordingly, the non-linear regression yielded empirical values for the initial adsorption rate (a) and Elovich empirical constant (b), as shown in Table 4. In alignment with the literature, Wu et al. [45] reported the suitability of the Elovich model to simulate chemical gas/solid adsorption associated with high surface coverage. Elovich model can be presented by equation (13).

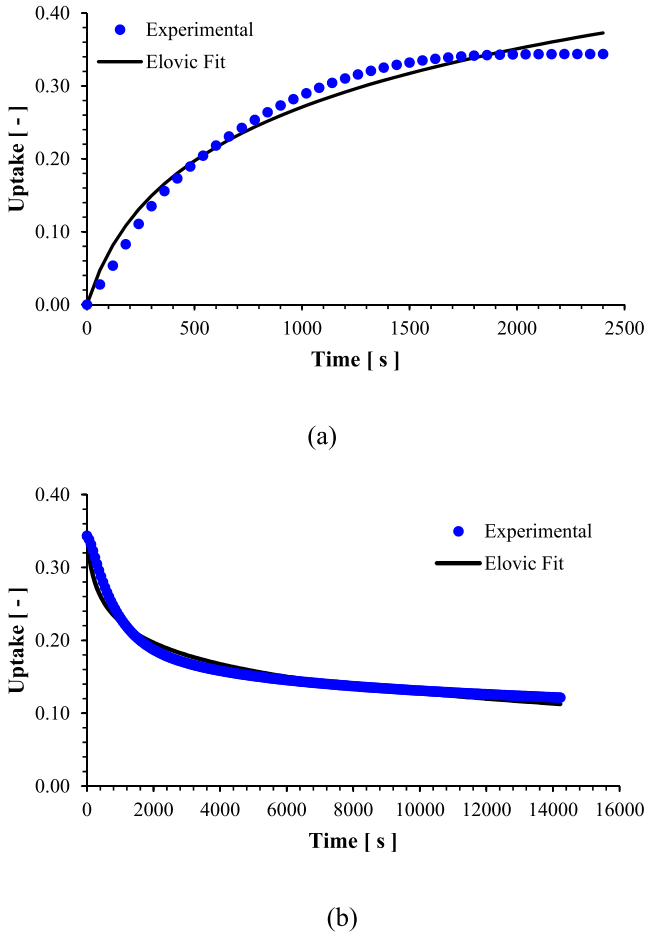

Fig. 10. Kinetic Elovich model compared to the experimental data at 25C (a) adsorption and (b) desorption.

Table 4
The empirical coefficient for the Elovich adsorption & desorption kinetic model.

Coefficient	Values		Units
	Adsorption	Desorption	
a	9.5×10^{-04}	6.2×10^{-04}	$kg_{ethnol}/kg_{silica}.s$
b	7.9	23	kg_{ethnol}/kg_{silica}
R^2	0.98	0.96	

$$q_t = \frac{1}{b}\ln(1 + abt) \tag{13}$$

Fig. 11 shows the desorption kinetics at different temperatures following the adsorption at 25 °C and 90 % partial pressure. It can be observed that the desorption rate increases by increasing the desorption temperatures as the thermal regeneration leads to faster mobility of ethanol molecules.

3.6. Theoretical cyclic performance

Fig. 12 presents the theoretical adsorption cycle for the silica gel/ethanol pair superimposed on the experimentally measured isotherms. This cycle's adsorption, evaporation, desorption, and condensation temperatures are 25, 0, 55, and 25 °C, respectively. The desorption temperature of 55 °C was chosen to represent the low-temperature heat available by PV/T and EVs. The theoretical net cyclic uptake at the material level for these operating conditions was $\Delta q = 2.32\% kg/kg_{ads}$, which represents the distance 2–3 or 1–4. The potential cooling capacity at the material level corresponding to such uptake is $q_{cooling} = \Delta q \times h_{fg} = 22kJ/kg_{ads}$; where h_{fg} symbolize the heat of vaporization at the given evaporator temperature. Based on the cyclic ethanol uptake and heat of adsorption, the potential cyclic regeneration heat required at the material level is $q_{regen} = \Delta q \times E_a/M = 22.6kJ/kg_{ads}$; where M symbolizes the molecular weight of ethanol. The theoretical coefficient of performance (COP) at the material level for silica gel/ethanol is 0.97, the ratio between the cooling and the regeneration energy. It is noteworthy that the cooling energy, regeneration energy, and COP are expected to show lower values when including the actual thermal behavior of the adsorption beds, evaporator, and condenser heat exchangers. Compared to the research that was done by Freni et al. [46], it was found that the cooling COP of composite LiBr/silica/methanol and LiBr/silica/ethanol pairs were 0.53 and 0.59, respectively.

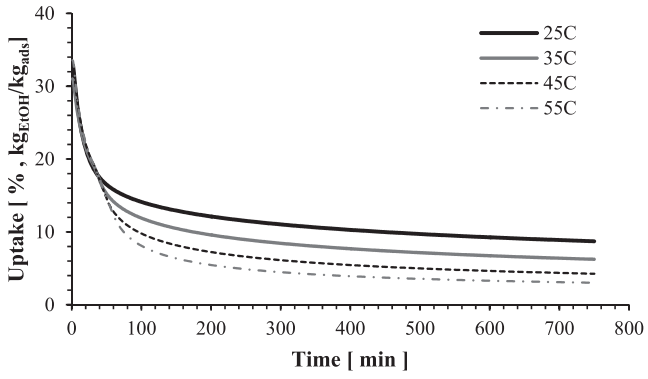

Fig. 11. Desorption kinetics at different temperatures started from equilibrium conditions at 90 % and 25 °C.

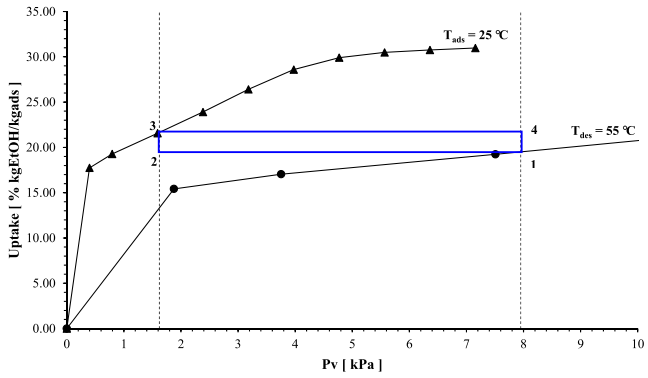

Fig. 12. Theoretical refrigeration cycle of silica gel/ethanol pair.

4. Conclusions and prospects

This study aimed to investigate and empirically model the adsorption characteristics of silica gel/ethanol pair under extended operating conditions to understand the influence of different operating temperatures on its performance. Therefore, silica gel structure stability, adsorption isotherm, adsorption kinetic, isosteric heat of adsorption, adsorption diffusion energy, and the theoretical cyclic performance at the material level were investigated. The findings of this study can be concluded as below.

- The repeatability experimentation showed no visible loss in the ethanol uptake over 10 consecutive adsorption/desorption cycles between 0 % and 90 % pressure ratio swing. The ethanol uptake varied from 12 % to 34 % during that cyclic operation, representing 22 % net cyclic uptake, with the adsorption rate considerably higher than the desorption.
- The maximum equilibrium uptake of ethanol onto silica gel was 30–32 %, with 56–62 % of the maximum uptake occurring at 10 % P_e/P_s for all temperatures. The slowness of the ethanol physical mobility and the high chemical adsorption led to a degree of non-desorbed ethanol that decreased as the desorption temperature increased from 12.4 % at °C to 5.8 % at 55 °C.
- The adsorption/desorption showed high reversibility quantified by 1.01 % hysteresis resulting from a degree of ethanol condensation at 50–60 % P_e/P_s. Obtaining heat-of-adsorption higher than the heat-of-vaporization confirms such a degree of condensation.
- Amongst the investigated adsorption isotherm models, Langmuir was the most suitable, but the Dubinin-Radushkevich model was the least, which was confirmed while analyzing the heat of adsorption.
- The diffusion energy of the ethanol inside silica gel pores was 1.80×10^4 J/mol, while the isosteric heat of adsorption was 42.3×10^3 J/mol. The observed deficit between the diffusion energy and the heat of adsorption resulted in the slow molecule mobility along the capillary walls most recognized during the relatively slow desorption.
- The theoretical cyclic performance at the material level showed the potential of the silica gel/ethanol pair to generate cooling of 22 kJ/kg_{ads} and the corresponding regeneration heat of 22.6 kJ/kg_{ads} with a relatively high COP of 0.97.

The developed understanding in this article is a stepping-stone towards further numerical and experimental investigation for silica gel/ethanol at the component and system levels, aiming to utilize ultra-low-temperature heat sources in EVs and PV/Ts application areas.

Declaration of Competing Interest

The authors declare that they have no known competing financial interests or personal relationships that could have appeared to influence the work reported in this paper.

Data availability

The data that has been used is confidential.

References

[1] G. Gediz Ilis, H. Demir, Influence of bed thickness and particle size on performance of microwave regenerated adsorption heat pump, Int. J. Heat Mass Transf. 123 (2018) 16–24, https://doi.org/10.1016/j.ijheatmasstransfer.2018.02.063.
[2] G. Gediz Ilis, et al., A new adsorbent bed design: Optimization of geometric parameters and metal additive for the performance improvement, Appl. Therm. Eng. 162 (2019), 114270, https://doi.org/10.1016/j.applthermaleng.2019.114270.
[3] W.D. Chen, K.J. Chua, Parameter analysis and energy optimization of a four-bed, two-evaporator adsorption system, Appl. Energy. 265 (2020), 114842, https://doi.org/10.1016/j.apenergy.2020.114842.
[4] A. Mahesh, S.C. Kaushik, Solar adsorption refrigeration system using different mass of adsorbents, J. Therm. Anal. Calorim. 111 (1) (2013) 897–903, https://doi.org/10.1007/s10973-012-2264-z.
[5] Gediz Ilis, G., H. Demir, and B.B. Saha, Innovative approach in adsorption chiller: Combination of condenser-adsorber for improving performance. Appl Therm Eng. 192 (2021) 116958. Doi: 10.1016/j.applthermaleng.2021.116958.
[6] C. Denzinger, et al., Toward sustainable refrigeration systems: Life cycle assessment of a bench-scale solar-thermal adsorption refrigerator, Int. J. Refrig 121 (2021) 105–113, https://doi.org/10.1016/j.ijrefrig.2020.09.022.
[7] I.I. El-Sharkawy, et al., Adsorption of ethanol onto phenol resin based adsorbents for developing next generation cooling systems, Int. J. Heat Mass Transf. 81 (2015) 171–178, https://doi.org/10.1016/j.ijheatmasstransfer.2014.10.012.
[8] A. Rezk, et al., Investigation of Ethanol/metal organic frameworks for low temperature adsorption cooling applications, Appl. Energy 112 (2013) 1025–1031, https://doi.org/10.1016/j.apenergy.2013.06.041.
[9] I.I. El-Sharkawy, et al., Adsorption of ethanol onto parent and surface treated activated carbon powders, Int. J. Heat Mass Transf. 73 (2014) 445–455, https://doi.org/10.1016/j.ijheatmasstransfer.2014.02.046.
[10] Elsayed, A., et al. Adsorption low temperature cooling using activated carbon/ethanol working pairs. in The 5th International Conference on Applied Energy ICAE 2013. 2013. Pretoria, South Africa.
[11] Q. Cui, et al., Environmentally benign working pairs for adsorption refrigeration, Energy. 30 (2) (2005) 261–271, https://doi.org/10.1016/j.energy.2004.05.005.
[12] M. Li, et al., Experimental study on adsorbent of activated carbon with refrigerant of methanol and ethanol for solar ice maker, Renew Energy. 29 (15) (2004) 2235–2244, https://doi.org/10.1016/j.renene.2004.04.006.
[13] A.A. Askalany, et al., A review on adsorption cooling systems with adsorbent carbon, Renew Sust Energ Rev. 16 (1) (2012) 493–500, https://doi.org/10.1016/j.rser.2011.08.013.
[14] K.A. Rocky, et al., Recent advances of composite adsorbents for heat transformation applications, Therm Sci Eng Prog. 23 (2021), 100900, https://doi.org/10.1016/j.tsep.2021.100900.
[15] A. Grekova, L. Gordeeva, Y. Aristov, Composite sorbents "Li/Ca halogenides inside Multi-wall Carbon Nano-tubes" for Thermal Energy Storage, Sol. Energy Mater. Sol. Cells 155 (2016) 176–183, https://doi.org/10.1016/j.solmat.2016.06.006.
[16] Gagliano, A., et al. Effectiveness and constraints of using PV/Thermal collectors for heat-driven chillers. in 16th SDEWES. 2021. Dubrovnik, Croatia.
[17] W.D. Chen, K.J. Chua, Energy performance analysis and optimization of a coupled adsorption and absorption cascade refrigeration system, Appl. Energy 301 (2021), 117518, https://doi.org/10.1016/j.apenergy.2021.117518.
[18] B. Tashtoush, H. Qaseem, An integrated absorption cooling technology with thermoelectric generator powered by solar energy, J. Therm. Anal. Calorim. 147 (2) (2022) 1547–1559, https://doi.org/10.1007/s10973-020-10512-5.
[19] F. Bayrak, H.F. Oztop, F. Selimefendigil, Effects of different fin parameters on temperature and efficiency for cooling of photovoltaic panels under natural convection, Sol. Energy 188 (2019) 484–494, https://doi.org/10.1016/j.solener.2019.06.036.
[20] F. Bayrak, H.F. Oztop, F. Selimefendigil, Experimental study for the application of different cooling techniques in photovoltaic (PV) panels, Energy Convers. Manage. 212 (2020), 112789, https://doi.org/10.1016/j.enconman.2020.112789.
[21] F. Calise, et al., A novel solar-assisted heat pump driven by photovoltaic/thermal collectors: Dynamic simulation and thermoeconomic optimization, Energy. 95 (2016) 346–366, https://doi.org/10.1016/j.energy.2015.11.071.
[22] M. Mohanraj, J.D.A.P. Abraham, Environment friendly refrigerant options for automobile air conditioners: a review, J. Therm. Anal. Calorim. 147 (1) (2022) 47–72, https://doi.org/10.1007/s10973-020-10286-w.
[23] S. Maeda, et al., Critical Review on the Developments and Future Aspects of Adsorption Heat Pumps for Automobile Air Conditioning, Appl Sci. 8 (11) (2018) 2061, https://doi.org/10.3390/app8112061.
[24] S.M. Ali, A. Chakraborty, Thermodynamic modelling and performance study of an engine waste heat driven adsorption cooling for automotive air-conditioning, Appl. Therm. Eng. 90 (2015) 54–63, https://doi.org/10.1016/j.applthermaleng.2015.06.078.

[25] M. Verde, et al., Performance evaluation of a waste-heat driven adsorption system for automotive air-conditioning: Part II - Performance optimization under different real driving conditions, Energy. 115 (2016) 996–1009, https://doi.org/10.1016/j.energy.2016.09.086.
[26] M. Verde, et al., Performance evaluation of a waste-heat driven adsorption system for automotive air-conditioning: Part I - Modeling and experimental validation, Energy 116 (2016) 526–538, https://doi.org/10.1016/j.energy.2016.09.113.
[27] M. Verde, K. Harby, J.M. Corberán, Optimization of thermal design and geometrical parameters of a flat tube-fin adsorbent bed for automobile air-conditioning, Appl. Therm. Eng. 111 (2017) 489–502, https://doi.org/10.1016/j.applthermaleng.2016.09.099.
[28] S. Vasta, et al., Development and lab-test of a mobile adsorption air-conditioner, Int. J. Refrig 35 (3) (2012) 701–708, https://doi.org/10.1016/j.ijrefrig.2011.03.013.
[29] Verde, M., et al., Modelling of an adsorption system driven by engine waste heat for truck cabin A/C. Performance estimation for a standard driving cycle. Appl Therm Eng. 30 (13) (2010) 1511-1522. Doi: 10.1016/j.applthermaleng.2010.04.005.
[30] R. Habash, et al., Analysis of low-grade heat driven ethanol-silica gel adsorption chiller, Therm. Sci. Eng. Prog. 26 (2021), 101125, https://doi.org/10.1016/j.tsep.2021.101125.
[31] H. Demir, M. Mobedi, S. Ülkü, Microcalorimetric investigation of water vapor adsorption on silica gel, J. Therm. Anal. Calorim. 105 (1) (2011) 375–382, https://doi.org/10.1007/s10973-011-1395-y.
[32] N. Ayawei, A.N. Ebelegi, D. Wankasi, Modelling and Interpretation of Adsorption Isotherms, J. Chem. 2017 (2017) 3039817, https://doi.org/10.1155/2017/3039817.
[33] X. Chen, Modeling of Experimental Adsorption Isotherm Data. 6 (1) (2015) 14-22.
[34] H. Demir, M.A. Deveci, Comparison of Ultrasound and Conventional Technique for Removal of Methyl Orange by Luffa Cylindrica Fibers, Arab. J. Sci. Eng. 43 (11) (2018) 5881–5889, https://doi.org/10.1007/s13369-017-3050-9.
[35] Q. Hu, Z. Zhang, Application of Dubinin-Radushkevich isotherm model at the solid/solution interface: A theoretical analysis, J. Mol. Liq. 277 (2019) 646–648, https://doi.org/10.1016/j.molliq.2019.01.005.
[36] Chickos, J.S. and W.E.A. Jr., Enthalpies of Vaporization of Organic and Organometallic Compounds, 1880–2002. 32 (2) (2003) 519-878. 10.1063/1.1529214.
[37] Y. Grillet, F. Rouquerol, J. Rouquerol, Two-dimensional freezing of nitrogen or argon on differently graphitized carbons, J. Colloid Interface Sci. 70 (2) (1979) 239–244, https://doi.org/10.1016/0021-9797(79)90029-8.
[38] J. Rouquerol, S. Partyka, F. Rouquerol, Calorimetric evidence for a bidimensional phase change in the monolayer of nitrogen or argon adsorbed on graphite at 77 K. J Chem Soc, Faraday Trans 1. 73 (0) (1977) 306-314. Doi: 10.1039/F19777300306.
[39] L. Giraldo, P. Rodriguez-Estupiñán, J.C. Moreno-Piraján, Isosteric Heat: Comparative Study between Clausius-Clapeyron, CSK and Adsorption Calorimetry Methods, Processes. 7 (4) (2019) 203, https://doi.org/10.3390/pr7040203.
[40] L. Pingan, L. Junpeng, W. Mengjun, Adsorption of ethanol molecules on the Al (1 1 1) surface: a molecular dynamic study, R. Soc. Open Sci. 6 (2019), 181189, https://doi.org/10.1098/rsos.181189.
[41] V. Orazi, et al., DFT study of ethanol adsorption on CaO(0 0 1) surface, Appl. Surf. Sci. 500 (2020), 144254, https://doi.org/10.1016/j.apsusc.2019.144254.
[42] Z. Sedlaček, Isosteric adsorption heats in correlation with activation energy of diffusion, Dept. Phys. Chem, Inst Chem Techl. (1974).
[43] Y. Sun, et al., Tunable LiCl@UiO-66 composites for water sorption-based heat transformation applications, J. Mater. Chem. 8 (26) (2020) 13364–13375, https://doi.org/10.1039/D0TA03442H.
[44] J. Wang, X. Guo, Adsorption kinetic models: Physical meanings, applications, and solving methods, J. Hazard. Mater. 390 (2020), 122156, https://doi.org/10.1016/j.jhazmat.2020.122156.
[45] F.-C. Wu, R.-L. Tseng, R.-S. Juang, Characteristics of Elovich equation used for the analysis of adsorption kinetics in dye-chitosan systems, Chem. Eng. J. 150 (2) (2009) 366–373, https://doi.org/10.1016/j.cej.2009.01.014.
[46] A. Freni, et al., Comparative analysis of promising adsorbent/adsorbate pairs for adsorptive heat pumping, air conditioning and refrigeration, Appl. Therm. Eng. 104 (2016) 85–95, https://doi.org/10.1016/j.applthermaleng.2016.05.036.